Chapter 4
Wear Mechanisms

Wear is a damage of a surface in contact with another one, which results in the formation of *fragments* (or *debris*) that leave the tribological system. Wear may cause direct failure, may reduce tolerances and surface finish, or induce a surface damage that is responsible for the subsequent failure of the component (most often by fatigue).

The characteristics of the relative motion between two bodies in contact define the *wear processes*. Some examples are schematically shown in Fig. 4.1. If the bodies' slide one over the other, the resulting wear process is *sliding wear*. If they roll one over the other, the resulting wear process is *rolling wear*. A *rolling-sliding wear* is obtained if the two types of motion are superimposed. When a reciprocating sliding is present with very small displacement, the resulting wear process is called *fretting*. When one of the two bodies consists in one or more hard particles that abrade a softer surface, wear is called *abrasion by hard, granular material*. If a fluid carries such abrading particles, wear is called *erosion*.

Despite the high number of wear processes encountered in practice, the investigation of wear damage is facilitated by the observation that each wear process is determined by the action of a predominant *wear mechanisms*, and the wear mechanisms are only four [1, 2]:

(1) adhesive wear;
(2) tribo-oxidative wear;
(3) abrasive wear;
(4) wear by contact fatigue.

An understanding of the four wear mechanisms is crucial to properly control every wear process. This control can be done in the designing stage, when it is possible to recognize in advance the acting wear mechanism. This control can be also done subsequently, when there is the need to re-design a tribological system after a wear induced failure. To achieve this task, a proper *failure analysis* is required and this can be carried out only if the main wear mechanisms are correctly understood. In this chapter the four wear mechanisms will be described, while in the next chapter the salient features of the main wear processes will be outlined. At the

© Springer International Publishing Switzerland 2015

G. Straffelini, *Friction and Wear*, Springer Tracts in Mechanical Engineering,
DOI 10.1007/978-3-319-05894-8_4

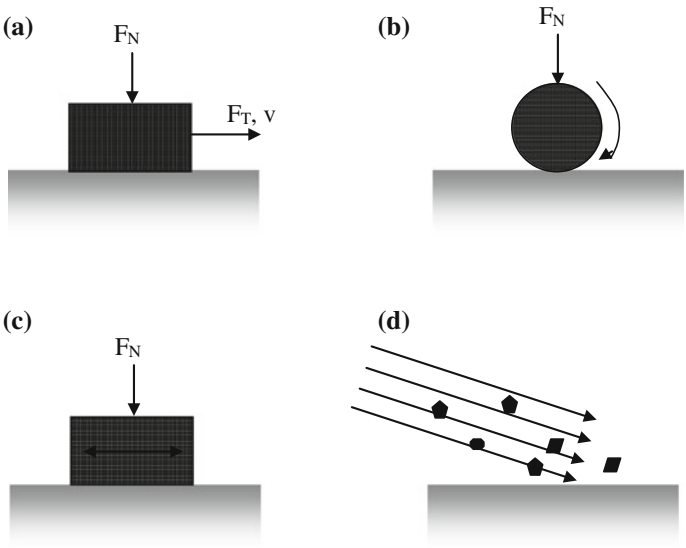

Fig. 4.1 Examples of types of relative motion between bodies in contact and the related wear processes: **a** sliding wear; **b** rolling wear; **c** fretting wear; **d** hard particles transported by a fluid: erosive wear (erosion)

end of this chapter, the main wear testing procedures able to simulate the different wear mechanisms are also outlined.

4.1 Adhesive Wear

Adhesive wear takes place when the adhesion forces between the contacting asperities exert a predominant role in the formation of wear fragments. Historically, this mechanism is described by the *theory of Archard*, even if the current interpretation has been improved, thanks to the developments in the observation of the fragments and worn surfaces that have lead to a better understanding of the phenomena that are actually involved.

In the study of adhesive wear, it is useful to distinguish between wear of ductile materials (like most metals and polymers above their glass transition temperature) and wear of brittle materials (such as ceramics and polymers below their glass transition temperature).

4.1.1 Adhesive Wear of Ductile Materials

In ductile materials, plastic junctions form at the contacting asperities during sliding (Fig. 1.11). As mentioned in Sect. 2.5, adhesion takes place at the junctions that in

some cases may be more resistant than the bulk. As a consequence, the tangential displacement at some asperities may be due to fracture in the asperity bulk rather than by shearing at the interfaces. Such a fracture results in the formation of a loose wear fragment. As schematized in Fig. 4.2, the total *wear volume*, is given by: $V = h A_n$, where h is the *depth of wear*, and the *wear rate* is given by the ratio between the wear volume and the sliding distance, s: $W = V/s$. Since wear involves the contacting asperities, W is proportional to the contact area A_r:

$$W = K_{ad} \cdot A_r = K_{ad} \cdot \frac{F_N}{H} \tag{4.1}$$

having used Eq. 1.17 to express A_r. If the two materials in contact have different hardness values, H in Eq. 4.1 is that of the softer material, since it determines the extension of A_r and produces the wear fragments. Following the Archard's view, the constant K_{ad} (called the *wear coefficient for adhesive wear*) is representative of the fraction of junctions that give rise to the formation of a wear fragment, i.e., it provides the probability that a junction will form a wear fragment [3, 4].

However, it has been experimentally observed that during sliding different phenomena occur at the asperity contacts, and they have to be taken into account to properly understand the wear mechanism and, in particular, to clarify the meaning of the wear coefficient. First of all, the repeated plastic deformations at the asperities may induce local low-cycle fatigue damage or an accumulation of plastic deformation by ratcheting (see Sect. 2.1) [5, 6]. These processes involve quite extensive areas in the sub-surface contact regions and contribute to the material weakening. Hence, they lead to the formation of a wear fragment once a critical damage is attained. The intensity of the applied stresses is proportional to the local adhesion forces, and therefore to W_{12}. The resistance of the material to low cycle-fatigue/ratcheting is proportional, to a first approximation, to the material hardness, H. The adhesive wear coefficient, K_{ad}, can be thus considered proportional to the ratio W_{12}/H and therefore to friction coefficient (see Eq. 2.10a). The general validity of such observations is confirmed by the results reported in Fig. 3.6a and b, which refer to

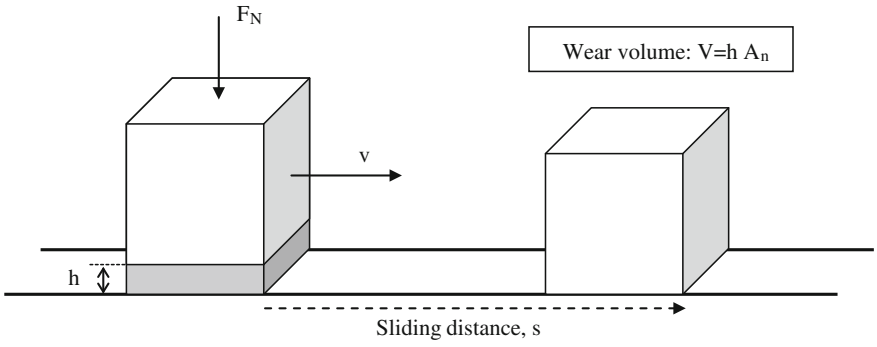

Fig. 4.2 Definition of sliding distance and wear volume

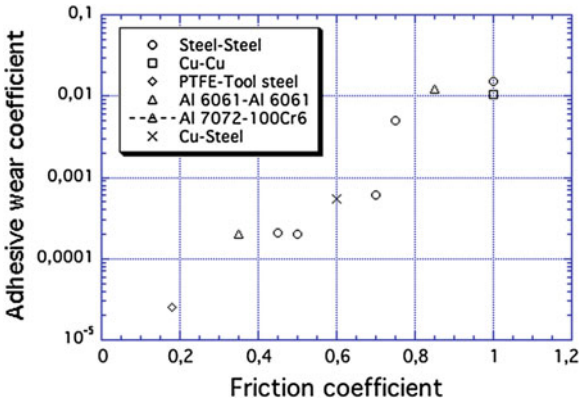

Fig. 4.3 Relationship between experimental adhesive wear coefficient and friction coefficient in the case of different material pairs. The experimental data were obtained from tests conducted in order to have the sliding adhesive wear (in the case of different materials, the wear coefficient of the softest material is shown)

the wear behaviour of different solid lubricants. Additional results are displayed in Fig. 4.3 for different materials pairs (in each case, the tests were carried out in sliding condition chosen to obtain adhesive wear). Following the arguments outlined in Chaps. 1 and 2, the adhesive wear coefficient is then reduced as the tribological compatibility of the mating materials is decreased and their hardness is raised.

The typical morphology of the worn surfaces, the sub-surface damaged regions and the wear fragments are shown in Fig. 4.4. The reported observations refer to a titanium alloy (Ti-6Al-4V) after dry sliding against a steel counterface [7, 8]. The occurrence of large shear plastic deformation (by ratcheting/low cycle fatigue) at the asperities can be clearly appreciated in Fig. 4.4a. The cross section in Fig. 4.4b shows that plastic shearing involves the sub-surface regions too. This figure also shows the formation of a surface deformed scale that is about to leaving the tribological system, i.e., to *delaminate* as it is often said. The morphology of the wear fragments is finally shown in Fig. 4.4c.

In most cases, other phenomena taking place in the contact region gain in importance in determining the friction and wear behaviour, and the whole picture becomes more complex. For example, quite often wear fragments remain entrapped between the contacting surfaces before leaving the tribological system. Therefore, they can transfer on to the counterface (forming, as already seen, a transfer layer) or, in the case of prolonged sliding, they can mix with other fragments from the counterface, forming a *mechanically-mixed layer* on the surface of the bodies in contact. In such cases, friction and wear are modified. It is almost impossible to predict them on the basis of simple considerations (such as the W_{12}/H ratio), and it is thus necessary to carry out experimental tests to achieve the required information.

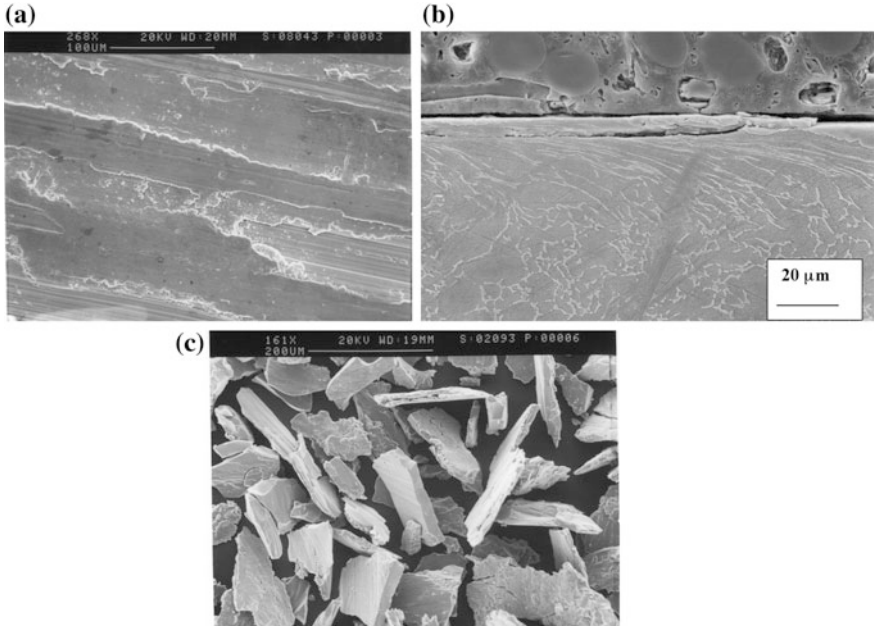

Fig. 4.4 Ti-6Al-4V sliding against a steel counterface. **a** Worn surface showing large shear plastic deformations at the asperities; **b** plastic shearing in the sub-surface region; **c** scale morphology of the metallic fragments [7, 8]

Although the theory of Archard states that adhesive wear is restricted to the body with the lowest hardness, the wear of the tribological system is in general given by the sum of the wear volumes of the two bodies in contact. If one body is much softer than the other, it contributes alone to wear and the hardest body in contact may also increase in weight (and volume) after sliding because of transfer phenomena. But if the two bodies have comparable hardness, both contribute to the total wear volume. In this case, Eq. 4.1 can be used to determine the wear volume of each body. Indicating with K_{ad1} and K_{ad2} the wear coefficient of material 1, the hardest one, and material 2, the softest one, respectively, from a number of experimental data Rabinowicz obtained that $K_{ad1} = 1/3\ K_{ad2}$ [9].

4.1.2 Adhesive Wear of Brittle Solids

A special case of adhesive wear occurs in brittle contacts (Sect. 1.1.4). The adhesive interaction at the contacting asperities, in fact, induces the appearance of a surface tensile stress during sliding, as described in Sect. 2.1. Such a stress can induce the formation of a wear fragment by brittle contact, if the material has sufficiently low fracture toughness [10]. Consider, for example, the contact between a sphere and a

plane. Combining Eqs. 1.7 and 2.1 and setting ν = 0.25 (the usual value of Poisson's ratio in the case of ceramic materials, which are typical materials that can give brittle contact), we get:

$$\sigma_t \cong \frac{p_{\max}}{6}(1 + 10\mu) \tag{4.2}$$

If a micro-crack of length c is present on the surface of the plane (see Fig. 1.6c), the surface tensile stress, given by Eq. 4.2, can produce brittle fracture if it reaches a critical value given by Eq. 1.10. Combining Eqs. 4.2 and 1.10, the condition for *adhesion-induced brittle contact wear* is given by:

$$p_{\max} \geq \frac{5.36 \cdot K_{Ic}}{\sqrt{\pi c} \cdot (1 + 10\mu)} \tag{4.3}$$

This mechanism of wear is common in ceramic materials, which are characterized by low values of K_{Ic}. In this case, c is closely related to the size of the crystalline grains, since defects, such as pores, are mainly located at the grain boundaries. For example, setting c = 10 μm, K_{Ic} = 2 MPa $m^{1/2}$ and μ = 0.4, we obtain that wear occurs when $p_{max} \approx 380$ MPa. An example of such a macroscopic brittle behaviour is shown in Fig. 2.14 (left side of the picture). The corresponding values of wear rate and friction coefficient are quite large. The fragments have a blocky or plate-like shape on the scale of the grain size.

If the applied pressure is lower than the critical value given by Eq. 4.3, massive wear by brittle contact (and fragmentation) does not occur. Fragmentation is rather confined at the asperities, and the fragments are compacted to form surface scales able to support the applied load (Fig. 2.14, right side). As a consequence, both wear rate and friction coefficient are relatively low. Wear debris are finer than the average grain size [11].

Equation 4.1 is often used to express the adhesive wear behaviour of brittle solids too. The experimental K_{ad}-values typically range between 10^{-8} and 10^{-2}. The highest values are attained when the applied stress is above the critical value.

4.2 Tribo-Oxidative Wear

Tribo-oxidative wear is due to the interaction of the surfaces with an environment containing oxygen. Tribo-oxidative wear is thus given by a combination of oxidative and mechanical actions at the contacting asperities. In general, it is accompanied by the formation of a surface oxide scale, which avoids the metal-to-metal contact at the asperities and may act as a sort of solid lubricant, thus reducing friction and wear. There are different situations that may lead to tribo-oxidative wear. First of all, it is convenient to distinguish between *tribo-oxidative wear at high temperatures*, and *tribo-oxidative wear at low sliding speed* [12].

4.2.1 Tribo-Oxidative Wear at High Temperatures

Tribo-oxidative wear at high temperatures may occur in two situations:

(1) at high sliding speeds, greater than 1 m/s in steels;
(2) when the contacting materials are exposed to high temperatures.

In both cases, surface temperature is sufficient to promote the *direct oxidation* of the asperities.

Consider first the direct tribo-oxidation at high sliding speeds. The model here presented is mainly due to the work by Quinn [13]. Oxidation is regarded to be activated by the contact flash temperature, T_f, and involves the contacting asperities. In the case of steels, T_f has to be greater than about 700 °C to trigger this type of wear (and the average surface temperature is greater than 300–400 °C). The oxide grows at the asperity tips and spalls off once a critical thickness, Z_c, is reached (about 10 μm in steel materials). The oxide breaking thus produces wear fragments and generates a fresh surface that can oxidize again, thus continuing the process. As the oxidation involves the contacting asperities, the wear rate, W, is directly dependent on the contact area, A_r. W can be expressed with the following equation [14]:

$$W = \frac{V}{s} = \frac{Z_c \cdot A_r}{v \cdot t_c} \tag{4.4}$$

where v is the sliding speed and t_c is the time required to reach the critical oxide thickness. In most cases, including the case of steels, oxidation follows a parabolic kinetics and then: $\Delta m^2 = k\ t$, where Δm is the mass increase per unit area due to the oxygen taken up to form the oxide, and k is the rate constant:

$$k = A \cdot \exp\left[-\frac{Q}{RT_f}\right] \tag{4.5}$$

where A is the Arrhenius constant, Q is the activation energy for oxidation (in steels: $A \approx 10^6$ kg/m^{4}s and $Q \approx 138$ kJ/mol [14]), R is the gas constant and T_f is the flash temperature. Δm is connected with the stoichiometry of the oxide that is formed. In the case of steels, it may be assumed that Fe_3O_4 is formed. Then, if a volume ΔV_{Fe} of iron is oxidized per unit area, $\Delta m = 2/3\ \Delta V_{Fe}\ \rho_{Fe}(M_{O2}/M_{Fe})$, where ρ_{Fe} is the density of iron, M_{O2} is the molecular weight of oxygen and M_{Fe} that of iron. Neglecting the volume expansion that occurs in oxidation, the oxide thickness, Z, is equal to the thickness of iron from which it originates, and thus equal to ΔV_{Fe}. As a consequence: $Z^2 = C^2\ k\ t$, where $C = (3M_{Fe})/(2M_{O2}\ \rho_{Fe}) = 3.4 \times 10^{-4}$ m^3/kg. Since t_c is given by: $Z_c^2/C^2\ k$, using Eq. 4.4 and considering $A_r = F_N/H$, it is finally obtained:

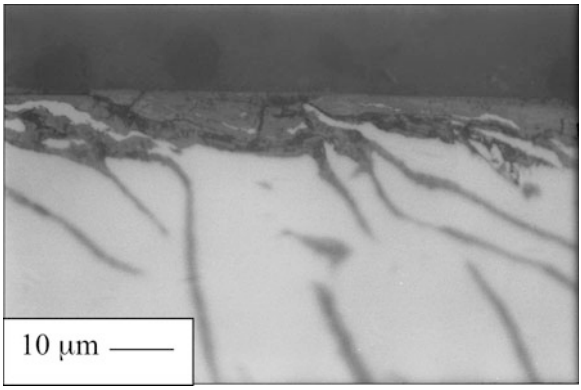

Fig. 4.5 Cross section of tribo-oxidized cast iron after sliding against a breaking pad [15]

$$W = \frac{C \cdot k}{v \cdot Z_c} \frac{F_N}{H} = \mathrm{K_{ox}} \frac{F_N}{H} \tag{4.6}$$

Equation 4.6 is similar to the relation 4.1, and the constant $\mathrm{K_{ox}}$ is called the *wear coefficient for tribo-oxidative wear*. $\mathrm{K_{ox}}$ is typically lower than 10^{-5} and strongly depends on the flash temperature.

As an example, Fig. 4.5 shows the cross section of a pearlitic cast iron after sliding against a braking pad [15]. The test simulated a severe braking condition, and the average contact temperature was greater than 500 °C. It is observed that direct oxidation took place in the surface and subsurface regions, with also some oxide penetration at the boundaries between the graphite lamellae and the cast iron matrix.

From a practical viewpoint, it is important to clarify the role exerted by the sliding parameters, such as normal load, sliding speed, and ambient temperature, on the tribo-oxidative wear behaviour of materials.

- $\mathrm{F_N}$. As shown by Eq. 4.6, as $\mathrm{F_N}$ is increased, W is increased too. But if $\mathrm{F_N}$ overtakes a critical value, the counterface may penetrate the oxide layer and destroy it by brittle fracture. In this way a metal-to-metal contact is established, and thus adhesive wear may occur.
- v. If sliding velocity is decreased and it is lower than a critical value (about 1 m/s for steels), the flash temperature is too low to trigger this wear mechanism. But if it is too high, greater than about 10 m/s for steels, *severe oxidation* occurs because of the high surface heating. The oxide becomes thick and plastic, and it flows on the metal insulating it and protecting it from wear.
- $\mathrm{T_0}$. If $\mathrm{T_0}$ is increased, $\mathrm{K_{ox}}$ is also increased because of the increase in flash temperature. However, an excessive temperature rise may cause a softening of the substrate that becomes unable to conveniently sustain the protective oxide layer. A transition to adhesive wear may thus occur, with a consequent increase in the wear rate.

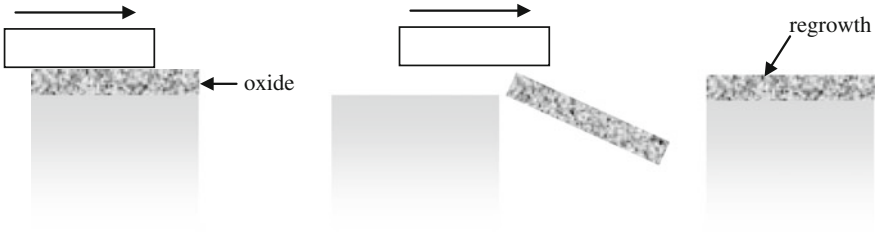

Fig. 4.6 Schematic of the oxidation-scrap-reoxidation mechanism, which occurs when ambient temperature is high

A particular situation takes place in case of *repeated sliding*. A typical example is given by the hot-rolling rolls (and hot working tools, in general). The surfaces undergo oxidation during the contact with the hot strip and, most of all, a general oxidation during the *out-of-contact* periods, due to environmental oxygen and also the vapour produced by cooling water. During the subsequent sliding contact the oxide scale can be then removed (partially or totally) and fresh metal is exposed to the environment for a reoxidation. This wear mechanism is called *oxidation-scrape-reoxidation*, and a schematic is shown in Fig. 4.6 [16]. The wear rate depends on the oxide growth kinetic, and therefore on the surface temperature reached during the in contact and out-of-contact periods (in between T_s and T_0). If the ambient temperature is quite high, the oxide formed during the out-of-contact periods can be sufficiently thick and can be only partially removed during the subsequent contact. In such a case, this type of tribo-oxidative wear is rather similar to the wear encountered at high sliding speeds (with severe oxidation), and it is therefore quite mild in nature.

4.2.2 Tribo-Oxidative Wear at Low Sliding Speed

Experience shows that tribo-oxidative wear, with evidence of oxide particles in the wear fragments, can take place even at low sliding speeds, i.e., when the flash temperature is not sufficient to trigger the direct oxidation of the asperity tips. It is particularly important in the case of reciprocating sliding, when wear fragments can be easily retained between the surfaces in contact. This type of tribo-oxidative wear has been extensively investigated by Stott [16]. The proposed model is shown in Fig. 4.7. Wear proceeds through the following steps:

(a) At the contacting asperities, metallic fragments are generated by adhesive wear. Some may leave the tribological system and some may remain trapped between the mating surfaces;
(b) Such fragments are strain-hardened, fractured, oxidized (oxidation is activated by the very high surface area and the high density of surface defects) and agglomerated;

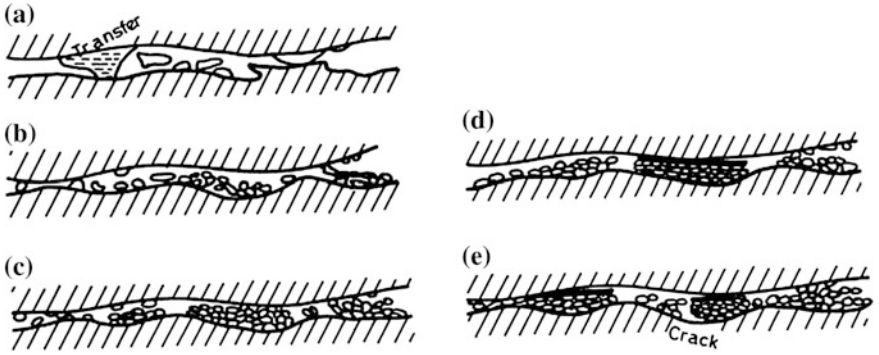

Fig. 4.7 Tribo-oxidative wear at low sliding speed: schematic representation of the Stott model (see text for details) [16]

(c) If the load and sliding conditions are intense, a tribological layer made of compacted scales is formed;
(d) If contact temperature is sufficiently high, the scales sinter and form a very protective *glaze* layer on the top;
(e) The possible brittle fracture of the scales (orthogonally to the sliding direction) leads to the generation of fragments that may remain in the contact region or leave the tribological system.

The intensity of wear is thus given by the attainment of a dynamic equilibrium between steps (a), (d) and (e). Depending on step (a), wear is often mixed, with the coexistence of metallic fragments (formed by adhesion), and oxidized fragments, formed at step (e). Equation 4.6 can be used to model the wear behaviour and K_{ox} is determined by experimental testing (such as pin-on-disc tests). In general, differently from the tribo-oxidative wear at high temperatures, wear rate decreases as surface temperature is increased, since temperature determine the conditions for a better formation of protective oxide scales.

An example of the typical morphology of the worn surfaces and the wear fragments is shown in Fig. 4.8. The pictures refer to a Ti-6Al-4 V alloy after dry sliding against a steel counterface [7]. On the worn surface (Fig. 4.8a), the presence of typical scales of compacted oxides (tribological layer) can be clearly observed. In some areas, such scales are also fragmented by brittle fracture, perpendicularly to the sliding direction. The wear fragments (Fig. 4.8b), are composed of very small equiaxed particles with a sub-micrometric size, which are oxide formed by the fragmentation of the compacted scales.

The role of ambient temperature in the tribo-oxidative wear at low sliding speed has been evidenced by Stott in a like-on-like reciprocating sliding test on a nickel alloy (with 20 % chromium), at temperatures between room temperature and 600 °C [16]. Figure 4.9 shows the results of the tests carried out at 15 N (6 h of sliding). Most of the oxide was NiO, and wear decreased with temperature since at

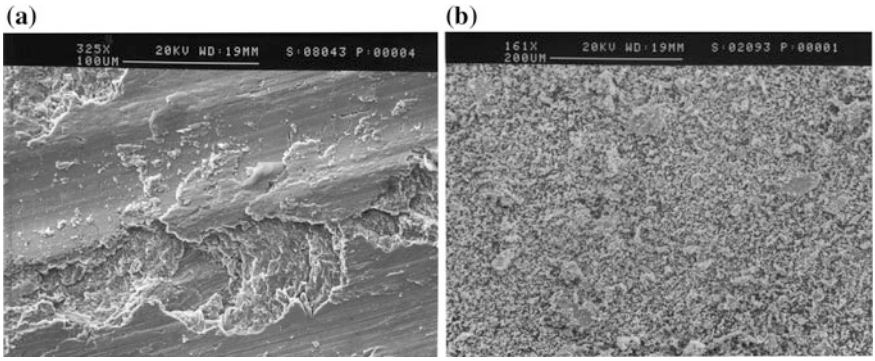

Fig. 4.8 Ti-6Al-4V sliding against a steel counterface. **a** Worn surface showing compacted oxide scales fractured perpendicularly to the sliding direction; **b** morphology of the wear fragments [7]

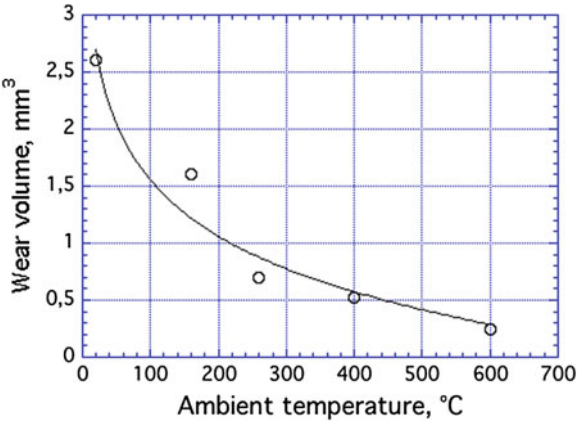

Fig. 4.9 Wear volume versus ambient temperature for like-on-like reciprocating sliding of a nickel alloy (Nimonic 80A) under a load of 15 N (modified from [16])

higher temperatures glaze layers developed on top of the compacted debris, leading to a more protective surface.

4.3 Abrasive Wear

As introduced in Sect. 2.8, there are two types of abrasive interaction: two-body and three-body abrasion. In the first case, a hard particle or a hard protuberance would plastically penetrate a softer counterface and groove it. Abrasive hard particles may be embedded in the material microstructure (such as in ceramic-reinforced composites, in steels or cast irons containing hard carbides, or in grinding wheels where the particles are held together by a specific bonding system), or may come from the surrounding environment (typical examples are the sand particles that contaminate

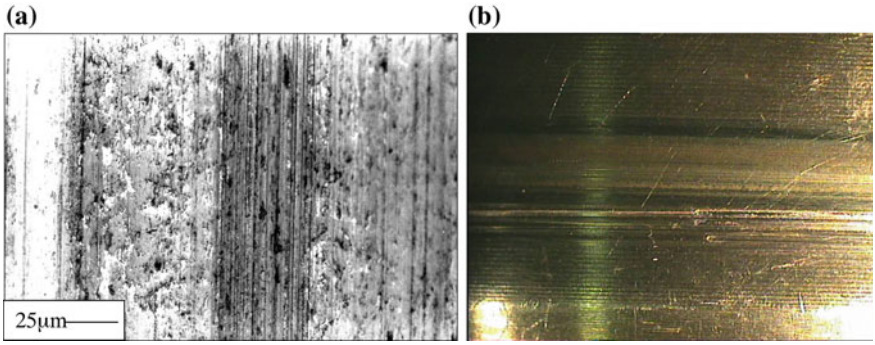

Fig. 4.10 **a** Cast iron disc abraded by the hard ingredients of a breaking pad (*vertical grooves*); **b** bronze surface abraded by contaminating sand particles (*horizontal grooves*)

tribological systems). Two examples are shown in Fig. 4.10. In the three-body abrasion, the hard particles trapped between two contacting surfaces are quite free to rotate and their action is thus limited. In any case, the abrasive interaction can occur only if the hardness of the hard particles is at least 20–30 % greater than that of the weakest surface. A special emphasis will be here given to two-body abrasion, which is a very severe form of wear. Also in this case, it is useful to distinguish between wear of materials with a ductile or brittle behaviour.

4.3.1 Abrasive Wear of Ductile Materials

The mechanism of two-body abrasioncan be represented as shown in Fig. 2.25. The cone represents the abrasive particle that plastically grooves the weakest surface during its movement. If all the plastically deformed material is removed, wear is by *microcutting* and it is maximum. If all the plastically deformed material flows to the sides of the groove, wear is by *microploughing* and it is zero, even if the surface can be severely damaged. A schematic of these two limiting cases is shown in Fig. 4.11.

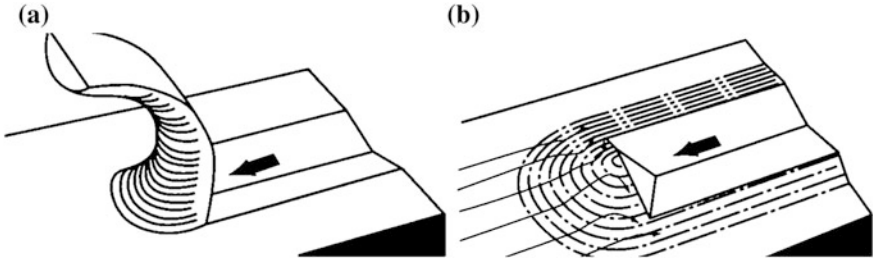

Fig. 4.11 Abrasive grooving by microcutting (**a**) and microploughing (**b**) (modified from [17])

Consider first the wear by microcutting. From the schematisation of Fig. 2.25 it is easily obtained that wear rate, W, is given by: $\frac{A_p \cdot s}{s} = A_p$, where A_p is the groove section generated by the cone in the direction of sliding ($A_p = r^2 tg\Theta$) and s is the sliding distance. At equilibrium: $F_N = p_Y \pi r^2/2 = H\pi r^2/2$ (only the front half of the moving cone supports the load), and thus [3, 4]:

$$W = \frac{2tg\Theta}{\pi} \cdot \frac{F_N}{H} \tag{4.7}$$

In general, however, microcutting and microploughing work together, and Eq. 4.7 has to be rearranged in the following way:

$$W = K_{abr} \cdot \frac{F_N}{H} \tag{4.8}$$

where K_{abr} is the *wear coefficient of abrasive wear*, given by:

$$K_{abr} = \Phi \cdot \frac{2tg\Theta}{\pi} \tag{4.9}$$

where Φ varies between 1 and 0. When $\Phi = 1$, wear is ideally by microcutting only. In this case $K_{abr} = \mu_{abr}$ (see Eq. 2.14) and the wear coefficient is very high. On the other hand, when $\Phi = 0$, wear is ideally by microploughing and $K_{abr} = 0$.

K_{abr} thus depends on the attack angle Θ and on the coefficient Φ, which are also interrelated. Θ depends on several factors including:

(1) the angularity of the particles (that is, if they are more or less rounded, and this depends on the type of the particles);
(2) the size of the particles;
(3) the hardness of the particles in relation to the hardness of the material being abraded;
(4) the replacement, or not, of the abrasive particles;
(5) the presence of any lubrication.

Obviously, the higher the angularity of the particles, the higher Θ. The attack angle also increases with increasing particle size, given that large particles may shatter during the contact and produce abrasive particles with sharp edges and thus high values of Θ. For example, it has been found that SiC particles in abrasive paper, with an average diameter of 16.3 μm, display an average attack angle of about 5°. If the average diameter increases to 57.3 μm, Θ increases to about 10°, and if the average diameter is 125 μm, Θ becomes approximately 15° [18]. In general, a plateau is reached around 150 μm, and Θ does not further increase if the particles size overtakes this limiting value. If, moreover, the antagonist were sufficiently hard, a rounding at the particles edges would most likely occur, thus reducing Θ. A particularly intense decrease in Θ is observed in the case of sliding without renewal of the abrasive particles: the transfer of the abraded debris on the

abrasive particles and even the detachment of the particles from the surface where they are embedded, can considerably reduce Θ. Conversely, in the presence of lubrication, flowing water included, the lubricant can remove the wear fragments of the abraded material, avoiding their accumulation that would block the abrasive action of the particles. In addition, lubricant reduces friction between the hard particle and the abraded surface, and these favours wear by microcutting [2].

The constant Φ mainly depends on the geometry of the abrasive particles (it increases as the attack angle is increased) and on the plastic properties of the worn material, in particular its ductility. The latter point may be interpreted considering that every abrasive interaction is characterized by a very intense plastic deformation, which can be also accumulated by ratcheting if the interaction is repeated. Such deformation can lead to the formation of a wear fragment by ductile fracture (even in the case of microploughing), if the ductility of the material is relatively low. In general, ductility is inversely proportional to hardness, and hence a dependence of Φ on the hardness of the abraded material has to be expected. In Fig. 4.12 such experimental dependence is shown for different metals and for high and low values of Θ. In the more general case of low Θ values, Φ is little dependent from hardness (and it is quite low, lower than 0.3) as long as hardness is lower than about 250 kg/mm^2. Therefore, in this region the *specific wear rate*, W/F_N, decreases as hardness is increased. But in the region 250–400 kg/mm^2, Φ strongly increases as hardness is increased. This means that the specific wear rate is almost independent from hardness (and it could also decrease as hardness is increased). If hardness is high, greater than, say, 400 kg/mm^2, Φ is, again, little dependent from hardness (and it is quite high, greater than 0.8). Also in this region, the specific wear rate is expected to decrease as hardness is increased further. The behaviour here described is typically found in many tribological systems and will considered in more detail in Sect. 5.4 [2].

In the case of three-body abrasion, the coefficient K_{abr} is much lower than in two-body abrasion, and it typically varies between 10^{-3} and 10^{-4}. This is due to the

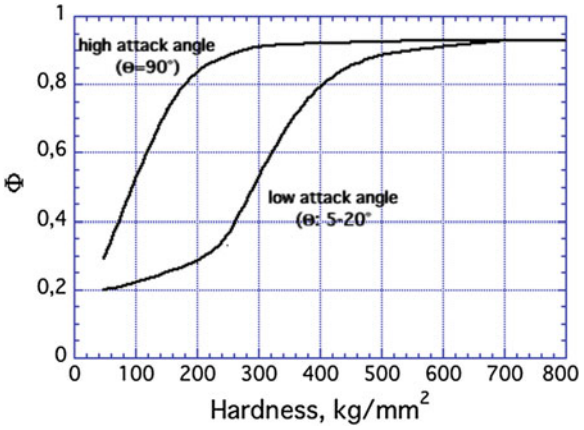

Fig. 4.12 Experimental dependence of parameter Φ (Eq. 4.9) with the hardness of (ductile) materials for high and low attack angles (data from [2, 18])

fact that the particles can roll between the bodies in contact (Fig. 2.24b), dissipating energy and also rounding their edges.

4.3.2 Abrasive Wear of Brittle Materials

In brittle materials, with low fracture toughness (K_{IC}), the abrasive interaction can produce a wear fragment by the Lawn and Swain mechanism, described in the Sect. 1.1.4 (see Fig. 1.7). In fact, the hard and angular particles may exert an indentation on the brittle surface over which they are sliding. The subsequent formation and propagation of lateral cracks (almost parallel to the surface of the abraded material) can lead to the formation of fragments of wear by spallation. If the hard particles are very rounded, they may induce a brittle fracture of the counterface following the Hertzian brittle contact (Fig. 1.6c).

Various models have been proposed to assess the wear rate in the case of abrasive wear by brittle fracture. In most models, W results directly proportional to the load applied by each abrasive particle, and inversely proportional to the material's hardness and fracture toughness. The model proposed by Evans and Marshall [19] is based on the Lawn and Swain mechanism and states that:

$$W = \alpha_3 \cdot \frac{F_N^{9/8}}{K_{Ic}^{1/2} \cdot H^{5/8}} \cdot \left(\frac{E}{H}\right)^{4/5} \tag{4.10}$$

where α_3 is an experimental constant. As an example, Fig. 4.13 shows the abrasive wear resistance (1/W per unit time) as a function of the so-called *abrasion parameter*, given by $H^{5/8} \cdot K_{IC}^{1/2}$. The experimental relationship is almost linear, in agreement with Eq. 4.10 (consider that the ratio E/H does not vary greatly among brittle materials). Such equation, however, should be used with caution. In fact, it

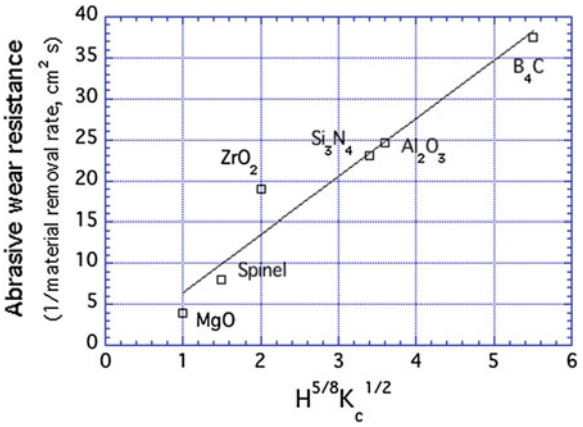

Fig. 4.13 Experimental relationship between the abrasive resistance and the abrasive parameter for different ceramic materials (modified from [19])

does not properly take into account the role of microstructure. In particular, weak grain boundaries could anticipate brittle fracture by favouring a grain boundary separation followed by grain ejection.

4.4 Wear by Contact Fatigue

The wear mechanisms considered so far are progressive in nature: in each case the material removal starts from the beginning of the contact and it continues almost linearly with time. In addition, the contact phenomena are always characterized by large plastic deformations. On the other hand, wear by contact fatigue is a typical *fatigue failure*: with the application of cyclic loading, a crack is nucleated and then it propagates up to the final fracture. This means that a wear fragment is produced after some cycles that correspond to the *fatigue life* of the loaded part. In addition, in most cases and depending on the intensity of the applied load, the overall damaging process takes place under small-scale plastic deformation, and the worn region appears macroscopically free from large plastic deformations. An example of surface fatigue damage in a bearing steel is shown in Fig. 4.14 [20].

In most cases, wear by contact fatigue occurs in non-conformal contacts, when at least one of the two bodies *rolls* over the other. In such cases, this wear mechanism is also called *rolling contact fatigue* (RCF). Wear involves the contact regions and is induced by the cyclic contact Hertzian stresses. The wear mechanism is rather complex, since it is influenced by numerous factors: contact stresses, lubrication regime (Λ-factor), sliding, material's properties (e.g. mechanical strength, fracture toughness, microstructural cleanliness), and residual stresses [21]. The phenomena involved in this wear mechanism are simply presented with reference to the operative lubrication regimes. Further details will be given in Sect. 5.3.

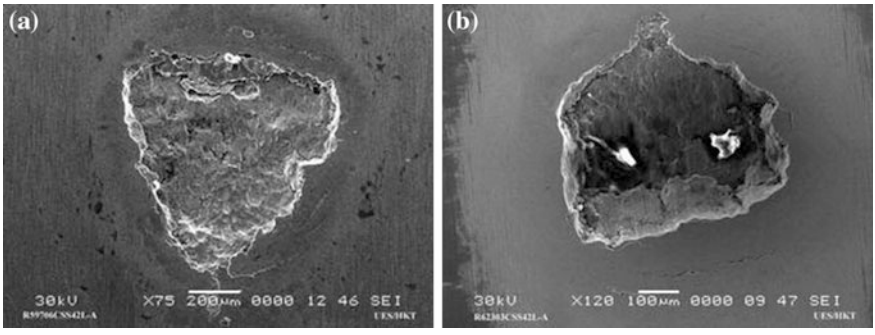

Fig. 4.14 Examples of surface fatigue damage in a CSS 42L bearing steel [20]

4.4.1 Contact Fatigue Under Fluid Film Lubrication

Under fluid film lubrication ($\Lambda > 3$), the asperities of the surfaces in contact do not touch and friction coefficient is very low, typically lower than 0.05. Assumed that the Hertz theory is applicable also in the case of cyclic loading, at each contact the surfaces are submitted to the stress distribution reported in Sect 1.1. The maximum shear stress, τ_{Max}, is located at a certain depth, z_m (see Table 1.1), and the sub-surface shear stress τ_{yz}, which is parallel to the surface (see Fig. 1.3c), changes direction during each contact (its maximum amplitude is $0.5p_{max}$).

Fatigue failure occurs by crack nucleation, crack propagation, and fracture. The sequence of phenomena leading to failure is shown in Fig. 4.15. Due to the cyclic loading, a subsurface crack nucleates after a number, N_n, of cycles. Crack nucleation typically occurs at areas with high stress concentration, i.e., non-metallic inclusions (oxides, sulphides), precipitates (carbides, nitrides) or pre-existing flaws. Alternatively, it may also occur at soft spots in the microstructure. Quite often, the nucleation stage is characterized by a local microstructural alteration, with dislocations build-up or transformation of retained austenite (this is quite typical in heat-treated steels), which induce a local hardening. Eventually, crack nucleation may be indirectly induced by carbide dissolution or other phenomena that are associated with local softening. Nucleation occurs at a depth close to z_m, where a critical combination of applied stress and microstructural defect is achieved (Fig. 4.15a). From a mechanical viewpoint, nucleation generally occurs after an elastic shake-down has been reached [22]. The number of cycles for crack nucleation, N_n, decreases as the contact load is increased, and therefore the subsurface stress, is

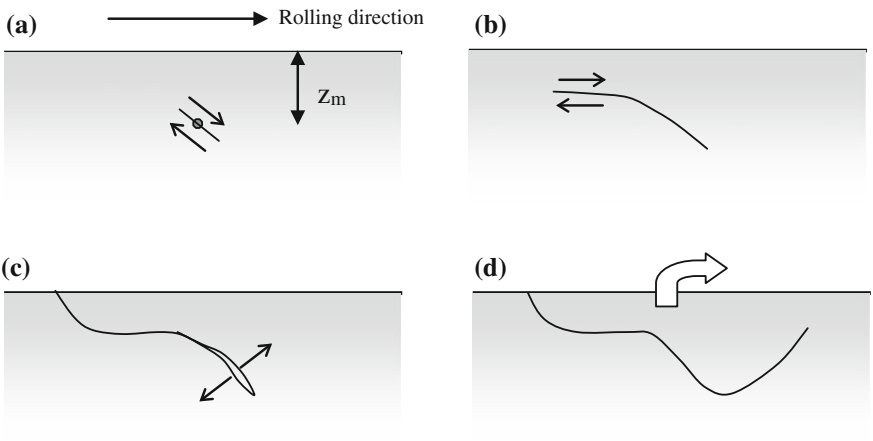

Fig. 4.15 Contact fatigue damage under fluid film lubrication. **a** Nucleation of a sub-surface crack at a depth close to z_m; **b** crack propagation towards the surface and then parallel to the surface; **c** crack branching to the surface (by ligament collapse) and oil pumping effect; **d** final formation of a large fragment by spalling

increased. If the elastic shakedown is overwhelmed, cracks can nucleate more easily by low-cycle fatigue.

After nucleation, the subsurface cracks propagate driven by the contact stresses. In general, the propagation is a mixed mode II (shear mode, which is predominant) and mode I (tensile mode) propagation. In a simplified view, it can be assumed that cracks initially propagate along the maximum shear stress forming an angle close to 45° with the surface. After some propagation, the cracks change direction and propagate parallel to the surface, driven by the τ_{yz} shear stress. Subsequently they propagate until the ligament between their tip and the surface fracture by plastic collapse [23]. These latter two events are schematized in Fig. 4.15b, c. From this moment, the lubricating fluid is entrapped in the crack, and exerts a *pumping effect*, which increases the driving force for crack propagation. The crack may then reach the surface also on the other side, thus producing a wear fragment by *spalling* (Fig. 4.15d). The wear fragment results quite large, typically greater than 100 μm in size.

The total number of cycles to failure, N, provides the fatigue life and is given by: $N = N_n + N_p$, where N_p is the number of cycles for crack propagation.

- N_n mainly depends on the microstructural features promoting crack nucleation. N_n thus increases as their density and size is decreased [24].
- N_p depends on microstructural defects that may offer energetically favourable paths for crack propagation and, most importantly, on microstructural strength and fracture toughness. In ductile materials, such as in most metals, as strength, i.e. hardness, is increased, the crack propagation rate is decreased, since the material strength in the plastic region at the crack tip is larger [25].

The parameter that is usually employed to quantify the stress intensity in the contact region is the Hertzian pressure, p_{max}, since both τ_{max} and τ_{xy} are directly proportional to it. As the Hertzian pressure is decreased, N is increased since both crack nucleation and propagation become more difficult. As known, fatigue failure is a statistical process, and N depends on the probability of finding a crack nucleation site close to the region with maximum stress. At a given pressure level, N thus depends on the maximum stressed volume, i.e., the volume of material at the surface where τ_{max} is greater than a given value (for example, greater than 0.8 τ_{Max}). The higher such a volume, the higher the probability of finding a critical defect, and thus the lower N.

In materials with a brittle behaviour, the picture somewhat changes. In this case the material matrix close to a defect possess low fracture toughness. Therefore, microstructural defects, such as flaws or pores, may be regarded as pre-existing cracks that are able to propagate very fast if the applied stress intensity factor is greater than a critical threshold. In addition, brittle materials display a particular behaviour when subjected to a point contact loading. As shown in Sect. 1.1.4, the surface radial tensile stress (Fig. 1.3a) may lead to brittle contact with the formation of C-cracks. The presence of a cyclic surface stress may favour such a crack nucleation, or cause the fatigue propagation of pre-existing cracks. As an example, Fig. 4.16 shows the crack network formed on the surface of a Si_3N_4 disc after a

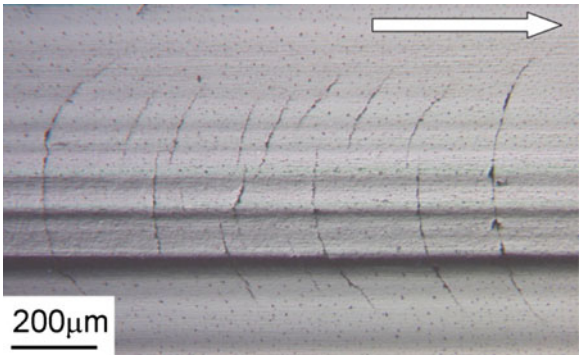

Fig. 4.16 Crack network on the surface of a Si_3N_4 disc after a rolling-sliding test period of 10 h (the *arrow* indicates the imposed sliding direction) [26]. Semi circular cracks are formed on the rear of the contact because of the additional contribution to the surface tensile stress given by friction (see Fig. 2.2)

rolling-sliding contact of 10 h against a hardened steel (contact pressure = 4.55 GPa; lubricant: emulsion of 5 % oil in water; recorded friction coefficient: 0.085) [26].

4.4.2 Contact Fatigue in Mixed and Boundary Lubrication Regime

The fatigue performance in fluid film lubrication can be considered as an upper limit, since it refers to a condition of optimum lubrication. A decrease in Λ induces a decrease in the contact fatigue resistance. If lubrication is mixed, a number of asperities are brought into repeated contact. As a consequence, crack nucleation at the surface is made easier, since the associated plastic deformation (that can be also characterized by asperity-scale ratcheting) may easily induce the formation of surface micro-cracks. They usually form a shallow angle with the surface because of some sliding at the asperity contacts that may be present even in the case of pure rolling if a torque is transmitted through the contact. Note that some micro-slip between two mating surfaces is almost always present even in case of free rolling, as shown in Sect. 2.10.

Geometrical discontinuities, such as grinding marks, are preferential sites for surface micro-crack nucleation. Cracks may then propagate towards the interior of the material if the local stress intensity factor exceeds the relevant threshold. Two main factors contribute to the stress intensity factor. The first one is represented by the contact stress. The presence of friction (which increases as Λ-factor is decreased) induces an increase in the local stress, and the Hertzian profile is also shifted to the surface (Fig. 2.3). The second one is due to the pumping effect exerted

by the lubricating oil. In this case, such effect starts immediately after surface crack nucleation. In non-conformal contacts the EHL pressure spike (Fig. 3.9) exerts an additional hydraulic pressure at the crack tip.

In most cases, after some propagation the cracks branch towards the surface because of the instability of shear propagation. A contact fatigue fragment is thus formed, which is relatively small, of the order of 10 μm in size. This phenomenon is often called *pitting* and it may anticipate failure by spalling if the Λ-factor is sufficiently low.

In brittle and hard materials, surface nucleation by plastic deformation is generally difficult. However, the high surface tensile stresses that depend on p_{max} and friction and are amplified by the EHL effect may lead to the nucleation of microcracks by asperity-scale fatigue or brittle fracture. Their propagation can produce severe damage by pitting.

4.5 Wear Testing

The coefficient of friction and all wear responses under the action of the different wear mechanisms, are not intrinsic materials properties, since they depend on the *tribological system*, i.e., on the mating materials, the type of contact, the surface characteristics of the mating bodies (including the possible presence of lubrication), and so on. Therefore, it is clear that for the determination of the realistic tribological behaviour of a given system, *field tests* are required. The tests should be then carried out on the actual system in service. Such tests, however, are expensive, long-term, complex and the results are often difficult to interpret, because it is very difficult to make out the influence of individual variables. For these reasons, it is preferred, in most cases, to perform laboratory tests in simpler configurations, such as:

(1) *bench tests* on the system of interest;
(2) accelerated *tests on single components* isolated from the real system;
(3) *simplified tests* that simulate the acting wear mechanism.

In passing from field tests, bench tests, accelerated component tests, and simplified tests, the relevant costs and test durations become generally lower. In addition, the test parameters are better controlled (specific standardized procedures have been also developed for many laboratory tests), and the obtained results can thus be more easily interpreted. Simplified tests can be conducted with adequate statistical confidence, and with the possibility of comparing the performance of different materials, even with literature data that refer to tests carried out under nominally identical or similar conditions. However, the simplified laboratory tests must be selected and performed with special care, and data have to be interpreted with caution, in order to transfer safely the obtained information to the real tribological system. A correct approach is based on the preliminary identification of the dominating wear mechanism responsible for the damage in operation, and on the

ability to carry out laboratory tests that wear the material specimens with the same mechanism.

A critical aspect of simplified laboratory tests regards the control of contact temperature. In fact, the adopted test specimens are often small in size in comparison to the real components they intend to simulate. Therefore, they may easily reach contact temperatures much different than those found in the real components (often higher but not always), even if the same tribological parameters (such as contact load and sliding velocity) are adopted. The different surface temperatures may induce a different wear mechanism (e.g. tribo-oxidation in place of adhesion). Its monitor and control (but adopting, for example, specific forced cooling systems, such as jets of compressed air) is thus paramount.

The data obtained from the laboratory tests may have a direct use in designing real tribological systems and configurations, like for instance, the sliding wear coefficients for dry sliding bearings, or the S-N curves for gears. In most cases, however, they are intended to produce a *ranking* between several candidate materials for a given application and relevant selection criteria. Consider that in many situations there is an uncertainty in using new materials, materials produced with a different process route or by different manufacturers, materials obtained by special coating techniques, and so on.

The available testing machines (*tribometers*) are very numerous and in most cases the test procedures are not governed by specific standards. This paragraph describes the main laboratory tribometers for basic simplified tests, which are able to simulate the different wear mechanisms. Table 4.1 lists the tribometers under consideration, together with the wear process and wear mechanism they are able to simulate. At the end of the paragraph, a short indication on the most common techniques for the examination of the wear products (wear debris and tracks) is given. In fact, in order to check for the validity of the executed tests, it is necessary to verify that the wear mechanism evidenced by the test sample is the same of that

Table 4.1 Simplified tribological tests with the related wear process and wear mechanisms that they are able to simulate

Test machine	Simulated wear process	Simulated wear mechanisms
Pin-on-disc	Sliding wear	Adhesive wear Tribo-oxidative wear
Block-on-ring	Sliding wear	Adhesive wear Tribo-oxidative wear
Disc-on-disc	Rolling-sliding wear	Contact fatigue Adhesion/tribo-oxidation
4 Balls	Rolling wear	Contact fatigue
Pin abrasion test (PAT)	High-stress abrasion	Abrasive wear
Dry-sand, rubber-wheel wear test (DSRW)	Low-stress abrasion	Abrasive wear

met in the real components. The same examination techniques are used for the failure analysis of the real components, a necessary step to establish which kind of test has to be performed.

4.5.1 Pin-on-Disc

This test setup is schematically shown in Fig. 4.17. The test configuration is constituted by a stationary pin with a cylindrical shape and a diameter of few millimetres, which is pressed against a rotating disc. The contact can be conformal or non-conformal. In the latter case, a sphere usually substitutes the pin. In the case of conformal contact, the edges of the contact are often rounded, in order to avoid (especially in lubricated tests) disturbing uncontrolled effects, due to stress concentration (see Fig. 1.4).

The control of the contact temperature is usually attained by placing one or two thermocouples in the pin, at a certain distance from the contact surface. The contact temperature is then evaluated using the relations introduced in Sect. 2.11. In this regard it should be noted that each region on the wear track on the disc gets in contact with the pin once per each revolution. If the disc is not able to dissipate the heat with sufficient efficiency, its temperature may rise continuously up to an equilibrium value. The contact temperature may thus become much higher than expected.

The depth of wear may be continuously recorded using a linear displacement transducer. In this case the measurement may also account for the wear contribution of the disc. Of course, the displacement of the transducer may be affected by thermal expansion of the pin due the frictional heating and this contribution has to be accounted for. Alternatively, wear may be measured by weighing the pin before and after each test (or at regular test intervals), and converting the mass loss to the volume loss using the density of the worn material. The wear of the disc is usually low. If necessary, it can be determined by obtaining the wear track profile, as measured with a profilometer. It is then possible to obtain a wear curve similar to

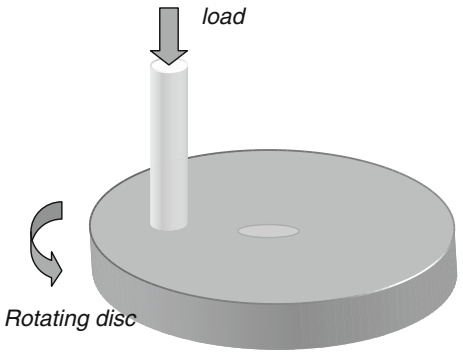

Fig. 4.17 Schematic of the pin-on-disc test

those shown in Fig. 5.1. With reference to the steady state stage, the wear rate (W), the specific wear coefficient (K_a) or the wear coefficient (K) can be evaluated quite easily. In the testing arrangement shown in Fig. 4.17, wear debris remain in the contact region. This may be important when simulating low-sliding speed tribo-oxidative wear. On the contrary, if the plane of the disc is vertical, all the debris falls away from the contact region. The test configuration has to be selected with respect to the wear mechanism to be simulated, and to the real contact conditions that need to be reproduced.

During each test it is also possible to follow the evolution of the friction coefficient. This is achieved by recording the tangential force required to restrain the pin. Such a measurement is very useful since, inter alia, it affords the possibility to detect the presence of transitions in the mechanism of wear that are typically evidenced by transitions in the friction coefficient. All the test procedures have been standardized in the ASTM G99-95 norm.

4.5.2 Block-on-Ring

In this test a stationary block is pressed against the outer surface of a rotating ring. As shown in Fig. 4.18, the contact can be conformal or non-conformal (at least at the beginning of the test). This test is very similar to the pin-on-disc test. It is usually preferred when there is the need to simulate sliding conformal contacts with large values of the nominal area of contact, and allowing the debris to be free to fall away the contact region. This type of test is also used to investigate lubricated wear, including the phenomenon of scuffing, in a non-conformal configuration, since it allows for the obtainment of high contact pressures.

In the case of conformal contact, a quite long running in stage is required to eliminate some unavoidable misalignments between the shaped block and the ring. Wear can be quantified by weighing the block and the ring before and after each

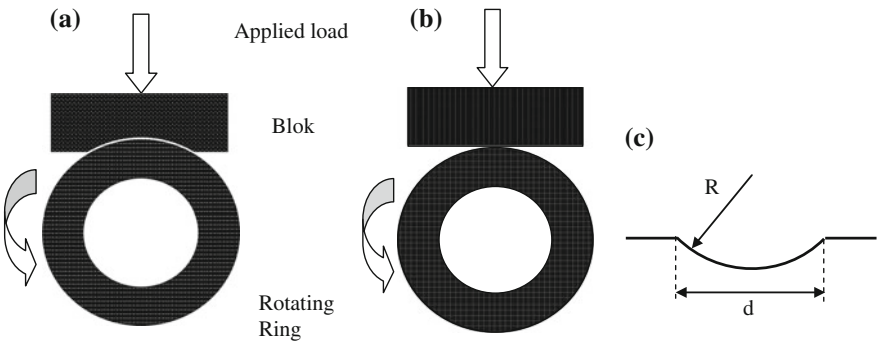

Fig. 4.18 Schematic of the block-on-ring testing rig. **a** Conformal contact; **b** non-conformal contact; **c** block wear volume determination using Eq. 4.11

test. In the case of non-conformal contact, the wear volume, V, is usually assessed by measuring the size of the wear track. The following relation can be used (see Fig. 4.18c for the meaning of the symbols):

$$V \cong \frac{d^3}{12R} L \tag{4.11}$$

The procedures to be followed for this type of test are given in ASTM G77-93.

4.5.3 Disc-on-Disc

In this test (also called *twin disc test*), two discs are in contact along a generatrix, realizing a non-conformal line contact. Figure 4.19a shows a schematic of the test setup. By changing the rotation velocity, rolling-sliding tests can be carried out at different percentages of sliding. The tests can be run in dry or lubricating conditions. In this case, lubricant can be taken to the contact region by means of a chain, which drags it from a container positioned below the specimens (Amsler-type tribometer; in this test, the discs have a diameter usually between 40 and 50 mm, and a height of 10 mm). The lubricant temperature is controlled and maintained on a fixed set value.

This type of test is mainly used to simulate wear by contact fatigue. By varying the test conditions (specimen geometry, surface roughness, applied loads and speeds), tests at different values of the lambda factor as well as of the Hertzian pressure can be conducted. By using crowned specimens, a point contact is established and very large contact pressures can be attained. The onset of fatigue

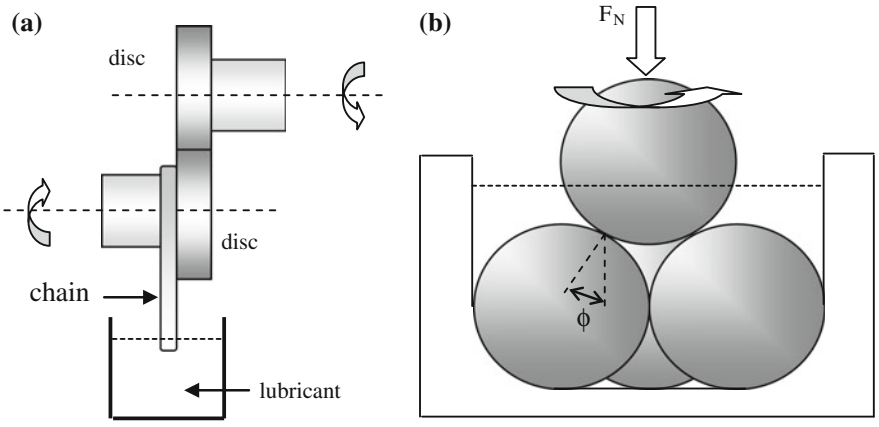

Fig. 4.19 Schematic side view of the **a** disc-on-disc testing rig (Amsler type), and **b** the 4-Ball tribometer

damage is usually determined in correspondence of a transition in the recorded friction coefficient, or by the appearance of noise or vibrations. In fact, if the wear fragments remain trapped between the bodies in contact, they induce an increase in the coefficient of friction and also induce vibrations in the system. The surface damage can be inferred by examining the surface state of the samples at regular intervals. Also this tribological test is widely used for studying the resistance of materials and lubricants to scuffing.

Different test configurations have been developed for reducing the running time. One example is the *four-roller test*, in which a cylindrical specimen is loaded by three counter discs (120° apart), giving three load applications for revolution.

4.5.4 Four-Ball Tribometer

The test setup is schematically shown in Fig. 4.19b. It realizes a point contact. The top rotating ball is kept in contact against the three stationary lower balls immersed in the lubricant. The load, F_N, is applied to the top ball and the load acting on each ball is then $F_N/3 \cos\phi$. For each rotation of the top ball produces three contacts with the lower balls that are typically made of an AISI 52100 steel. The eventual wear volumes of the balls are determined by measuring the wear scars on their surfaces. This type of test is mainly used to study the properties of lubricants (including their scuffing resistance). The standard test procedure is described in ASTM D 4172–94.

4.5.5 Dry-Sand, Rubber-Wheel Wear Test (DSRW)

This type of test is used to evaluate the tribological behaviour of materials under low-stress abrasion conditions. The test setup is schematically shown in Fig. 4.20. A rotating rubber-rimmed wheel slides against the surface of a specimen in the presence of abrasive particles, which are fed by gravity from a hopper. The

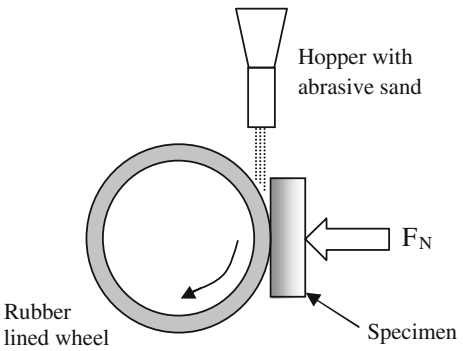

Fig. 4.20 Scheme of the DSRW test setup

procedure is described by the ASTM G65 standard. Sand particles (Ottawa sand, Fig. 5.17b) with a size of about 200 μm are used. In the procedure B, the applied load is 130 N and the sliding distance is 1430 m. Wear is determined by weighing the sample before and after the test. This allows obtaining the relevant wear rates and wear coefficients. As in the block-on-ring test, wear induces a continuous increase in the nominal area of contact.

The DSRW test can be modified to investigate the influence of specific parameters that may play an important role under particular tribological conditions. For example, the tests can be carried out using an abrasive slurry (ASTM B611) or in a corrosive environment.

4.5.6 Pin Abrasion Wear Test (PAT)

This type of test is suitable for the study of the high-stress abrasive behaviour of materials. The geometric configuration is similar to that shown in Fig. 4.17. A cylindrical pin (the sample to be studied) slides against an abrasive paper containing ceramic particles, typically alumina or silicon carbides. In order to avoid any interference between the abrading particles and wear debris, a spiral track is realized by moving the specimen towards the centre of the disc. Alternatively, a *pin on abrasive drum* test is used. In this test, a rotating cylinder is covered with an abrasive paper, and a pin is pressed against it whilst moving along a generatrix, in order to be continuously in contact with fresh abrasives. The evolution of wear is determined by periodically interrupting the test and weighing the pin.

4.5.7 Examination of the Wear Products

In order to understand the acting wear mechanism in a given tribological system, with the aim of validating the laboratory tests or in the failure analysis of real components, the observation of the *worn surfaces* (or *wear tracks*) is recommended. The observation of the wear fragments, if available, can be also very useful. Subsequently, the subsurface regions can be possibly observed, on carefully prepared metallographic cross-sections. The latter operation can be easily carried out in laboratory investigations on relatively small specimens, whereas it may be more difficult in the failure analysis of real components. Table 4.2 lists some of the most used techniques for the characterization of the worn surfaces, the wear fragments and the subsurface damaged regions.

In the case of *adhesive wear*, very useful information is obtained from the observations carried out using an Optical Microscope (OM), or in a Scanning Electron Microscope (SEM), especially in the Back-Scattered Electron (BSE) mode. As an example, Fig. 2.20a shows the wear surface of a steel after dry sliding against a bronze. The occurrence of adhesive wear is clearly demonstrated by the

Table 4.2 Most used techniques to characterize the wear damage

Worn surfaces (or, wear tracks)	Visual inspection	Optical microscopy	Electronic microscopy (SEM) equipped with micro-analysis (EDS)	Special techniques (such as XPS)
Wear fragments (o, debris)	Visual inspection	Optical microscopy	Electronic microscopy (SEM) equipped with micro-analysis (EDS)	X-ray diffraction (XRD). Transmission electron microscopy (TEM). Special techniques
Sub-surface regions	Optical microscopy	Microhardness profiles	Special techniques (such as SIMS)	

presence of transferred fragments that have a plate-like shape. The occurrence of transfer is also well evidenced by SEM observations in BSE mode or using the EDXS analysis (see, for example, Fig. 2.29).

Visual inspection and OM observations are very fruitful also for detecting wear by *tribo-oxidation*. As an example, Fig. 4.21 shows the OM planar view of the surface of a steel that underwent tribo-oxidative wear at low sliding speed. The presence of dark scales of compacted oxides can be clearly appreciated. In some cases such dark scales or fragments are simply detected by naked eye.

The presence of grooves on the wear surface of specimens or components is a clear indication of *abrasive wear*. Such grooves can be detected by OM, as shown in Fig. 4.10b. Such an operation can be easy accomplished when the grooves are all aligned along the same direction. It is much more difficult when they are produced by particles moving in different directions.

Figure 4.14 shows a steel surface damaged by *contact fatigue*, observed in a SEM. This technique allows observing surfaces with a high depth of focus, and it is

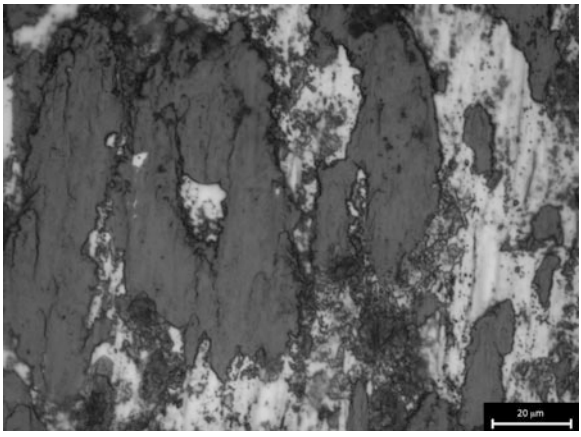

Fig. 4.21 OM observation of the wear track of a steel after tribo-oxidative wear [27]

therefore very useful in detecting spalled layers and pits produced by contact fatigue. An evidence of the occurrence of this kind of damage is also given by the limited, if any, presence of plastic deformations in the damaged areas. Indeed, in all other cases of wear damage, extensive plastic deformation is present.

References

1. K.H. Czichos, K.H. Habig, *Handbook Tribologie* (Vieweg, Reibung und Verlschleiss, 1992)
2. K.H. Zum Gahr, *Microstructure and Wear of Materials*, (Elsevier, New york, 1987)
3. E. Rabinowicz, *Friction and Wear Materials*, 2nd edn. (Wiley, New york, 1995)
4. I.M. Hutchings, *Tribology*, ed. by Edwald Arnold (London, 1992)
5. D.A. Rigney, L.H. Chen, M.G.S. Naylor, A.R. Rosenfield, Wear processes in sliding systems. Wear **100**, 199–219 (1984)
6. B.S. Hockenbull, E.M. Kopalinsky, P.L.B. Oxley, An investigation on the role of low cycle fatigue in producing surface damage in sliding metallic friction. Wear **148**, 135–146 (1991)
7. G. Straffelini, A. Molinari, Dry sliding wear of Ti-6Al-4V alloy as influenced by the counterface and sliding conditions. Wear **236**, 328–338 (1999)
8. G. Straffelini, A. Molinari, Mild sliding wear of Fe-0.2 %C, Ti-6 %Al-4 %V and Al-7072: a comparative study. Tribol. Lett. **41**, 227–238 (2011)
9. M.B. Peterson and W.O. Winer (eds) *Wear control handbook*, ASME (1981)
10. H.S. Kong, M.F. Ashby, Wear mechanisms in brittle solids. Acta Metall. Mater. **40**, 2907–2920 (1992)
11. K. Adachi, K. Kato, N. Chen, Wear map of ceramics. Wear **203–204**, 291–301 (1997)
12. G.W. Stachowiak and A.W. Batchelor *Engineering Tribology*, 3rd edn. (Elsevier, Amsterdam, 2005)
13. T.F.J. Quinn, Oxidational wear. Wear **18**, 413–419 (1971)
14. S.C. Lim, M.F. Ashby, Wear mechanism maps. Acta Mater. **35**, 1–24 (1987)
15. G. Straffelini, L. Maines, The relationship between wear of semimetallic friction materials and pearlitic cast iron in dry sliding. Wear **307**, 75–80 (2014)
16. F.H. Stott, The role of oxidation in the wear of alloys. Tribol. Int. **31**, 61–71 (1998)
17. D.A. Rigney (ed.) *Fundamentals of friction and wear of materials*, ASM (1981)
18. T. Hisakado, T. Tanaka, H. Suda, Effect of abrasive particle size on fraction of debris removed from plowing volume in abrasive wear. Wear **236**, 24–33 (1999)
19. A.G. Evans and D.B. Marshall, Wear Mechanisms in Ceramics, in Fundamentals of Friction and Wear of Materials, ed. by D.A. Rigney, ASM, pp. 439–452
20. H.K. Trivedi, N.H. Foster, L. Rosado, Rolling contact fatigue evaluation of advanced bearing steels with and without the oil anti-wear additive tricresyl phosphate, Tribol. Lett. **41**, 597–506 (2010)
21. S. Suresh, *Fatigue of materials*, 2nd edn. (Cambridge university press, Cambridge, 1998)
22. G. Donzella, M. Faccoli, A. Ghidini, A. Mazzù, R. Roberti, The competitive role of wear and RCF in a rail steel. Eng. Fract. Mech. **72**, 287–308 (2005)
23. Y. Ding, R. Jones, B.T. Kuhnell, Elastic-plastic finite element analysis of spall formation in gears. Wear **197**, 197–205 (1996)
24. D. Nelias, M.L. Dumont, F. Champiot, A. Vincent, D. Girodin, R. Fougeres, L. Flamand, Role of inclusions, surface roughness and operating conditions on rolling contact fatigue. J. Tribol.: ASME Trans **121**, 240–251 (1999)
25. N.A. Fleck, K.J. Kang, M.F. Ashby, The cyclic properties of engineering materials. Acta Metall. Mater. **42**, 365–381 (1994)

26. M. Hartelt, H. Riesch-Oppermann, I. Khader, O. Kraft, Probabilistic lifetime prediction for ceramic components in rolling applications. J. Eur. Ceram. Soc. **32**, 2073–2085 (2012)
27. G. Straffelini, M. Pellizzari, L. Maines, Effect of sliding speed and contact pressure on the oxidative wear of austempered ductile iron. Wear **270**, 714–719 (2011)